JACS
JOURNAL OF THE AMERICAN CHEMICAL SOCIETY
Article
pubs.acs.org/JACS

An Interface-Directed Coassembly Approach To Synthesize Uniform Large-Pore Mesoporous Silica Spheres

Minghong Wang,[†] Zhenkun Sun,[†] Qin Yue,[†] Jie Yang,[‡] Xiqing Wang,[†] Yonghui Deng,*[,†] Chengzhong Yu,[‡] and Dongyuan Zhao[†]

[†]Department of Chemistry and Shanghai Key Lab of Molecular Catalysis and Innovative Materials, the State Key Laboratory of Molecular Engineering of Polymers, and Advanced Materials Laboratory, Fudan University, Shanghai 200433, P. R. China

[‡]ARC Centre of Excellence for Functional Nanomaterials and Australian Institute for Bioengineering and Nanotechnology, The University of Queensland, Brisbane, QLD 4072, Australia

Supporting Information

ABSTRACT: A facile and controllable interface-directed coassembly (IDCA) approach is developed for the first time to synthesize uniform discrete mesoporous silica particles with a large pore size (ca. 8 nm) by using 3-dimensional macroporous carbon (3DOMC) as the nanoreactor for the confined coassembly of template molecules and silica source. By controlling the amount of the precursor solution and using Pluronic templates with different compositions, we can synthesize mesoporous silica particles with diverse morphologies (spheres, hollow spheres, and hemispheres) and different mesostructure (e.g., 2-D hexagonal and 3D face centered cubic symmetry), high surface area of about 790 m^2/g, and large pore volume (0.98 cm^3/g). The particle size can be tunable from submicrometer to micrometer regimes by changing the macropore diameter of 3DOMC. Importantly, this synthesis concept can be extended to fabricate multifunctional mesoporous composite spheres with a magnetic core and a mesoporous silica shell, large saturated magnetization (23.5 emu/g), and high surface area (280 m^2/g). With the use of the magnetic mesoporous silica spheres as a magnetically recyclable absorbent, a fast and efficient removal of microcystin from water is achieved, and they can be recycled for 10 times without a significant decrease of removal efficiency for microcystin.

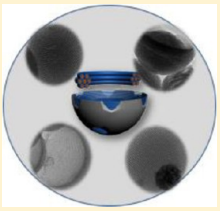

1. INTRODUCTION

The design of uniform colloidal spheres with tunable sizes, nanostructures, and functionalities is critical for applications in various fields, such as chromatography, catalysis, enzyme immobilization, and photonic bandgap (PBG) crystals.[1−12] Mesoporous silica spheres, as a family of novel zero-dimensional nanomaterials, have recently attracted increasing attention for their uniform and highly accessible mesopores, high surface area, large pore volume, and potential applications in drug delivery,[13−15] gene transfection,[16−18] catalysis,[19,20] adsorption of pollutants,[21−23] and so forth. Unfortunately, by using small surfactants (e.g., cetyltrimethylammoniabromide, CTAB) as the template, only MCM-41 type uniform mesoporous silica spheres can be directly synthesized, and they possess small pore size of around 2.0−3.0 nm.[24−26] The limitation of pore size can significantly hinder their applications where catalytically active nanoparticles (e.g., Pd and Pt nanocrystals) or biomacromolecules of large size need to be loaded or adsorbed/immobilized. Although the utilization of pore expanding agent (e.g., mesitylene, TMB) can enlarge the pore size,[27,28] it leads to mesoporous silica particles with irregular morphology or disordered mesostructures.[29−32] On the other hand, by using Pluronic triblock copolymers (PEO-*b*-PPO-*b*-PEO, e.g., P123 and F127) as templates, many research groups have devoted great effort to synthesizing mesoporous silica microspheres with large mesopores (>5.0 nm) through the solution-phase coassembly or aerosol-assisted solvent evaporation induced self-assembly (EISA) route. In this regard, Tian et al.[33] reported 400 nm sized SBA-15 particles with pore size of 12 nm through aqueous solution-phase synthesis using Pluronic P123 as the template, NH_4F as catalyst, and decane as a cosolvent and the morphology controlling agent. The particles are uniform in size and nearly spherical in shape, but the pore structure is limited to 2-D hexagonal symmetry. Recently, Gu et al.[34] attempted to synthesize large-pore mesoporous silica nanospheres (MSNs) by using mixed pore forming agents of cationic surfactants, *N*,*N*-dimethylhexadecylamine (DMHA) and Pluronic F127. It is found that the pore can be tunable in the range of 3.8−5.6 nm by increasing the amount of DMHA, while F127 molecules only serve as the particle growth inhibitor/dispersant and change the particle size of MSNs in the range of 80−140 nm. To date, it is difficult to produce highly uniform mesoporous microspheres by simply using Pluronic block copolymers as the templates due to the difficulty in controlling the coassembly process.[35−38] Consequently, it is highly urgent and important to develop new approach to synthesize uniform mesoporous materials with large pore size that can be used for applications involving large-size guest objects, such as immobilizing bioenzymes and loading metal nanoparticles for catalysis.

Three-dimensionally ordered macroporous (3DOM) materials, due to their periodic alignment of uniform, well-interconnected spherical cavities and diverse framework

Received: September 26, 2013
Published: January 13, 2014

   dx.doi.org/10.1021/ja4099356 | *J. Am. Chem. Soc.* 2014, 136, 1884−1892

compositions,[39−43] have attracted much attention for their applications for optics, energy conversion and storage, sensors, catalysis,[44−47] and so on. Recently, they have been used as a confined nanoreactor for the fabrication of monodisperse microspheres by utilization of their void cavities for deposition of the precursor solution and in situ conversion into the desired nanomaterials.[48−56] Yoo et al.[53] synthesized uniform zeolite microspheres through a controlled growth of zeolite using 3DOM carbon (3DOMC) as massively parallel reaction chambers. More recently, spherical ordered mesoporous carbon (OMC) nanoparticles with bimodal mesopores have been synthesized in the macropores of 3DOM silica through EISA method.[54] The continuous success in fabricating monodisperse microspheres suggests that the 3DOM materials can serve as a unique nanoreactor for producing various nanostructures with good size uniformity and structural regularity.

Herein, for the first time, we report a facile and controllable interface-directed coassembly approach to synthesize uniform discrete mesoporous silica particles with large pore size (ca. 8 nm) by using 3DOMC as the nanoreactor for the solvent evaporation induced coassembly of amphiphilic template molecules and silica source. By controlling the amount of the precursor solution introduced into the macropore cavities, ordered mesoporous silica particles with different morphologies (spheres, hollow spheres, and hemispheres), high surface area of about 790 m^2/g, and large pore volume (0.98 cm^3/g) can be synthesized. The particle size can be tunable from submicrometer to micrometer regimes by changing the macropore diameter of the 3DOMC template. The mesostructure of the mesoporous silica spheres can be varied from 2-dimensional (2-D) hexagonal (*P6m*) to 3-D face centered cubic symmetry (*Fm*3*m*) by using different Pluronic copolymers as the structure-directing agents. Interestingly, through preplacing a magnetic particle in each macropore of the 3DOMC template before introducing precursor solutions, novel mesoporous silica composite spheres with a magnetic core and mesoporous silica shell can be synthesized. The obtained magnetic mesoporous silica spheres have a large saturated magnetization of about 23.5 emu/g, high surface area (280 m^2/g). When we use the magnetic mesoporous silica spheres as an absorbent, a fast and efficient removal of microcystin from water can be achieved with help of a magnetic field. After easy regeneration by solvent extraction, the magnetic absorbents can be recycled without significant decrease in uptake of microcystin even after using for 10 times.

2. EXPERIMENTAL SECTION

2.1. Chemicals. Pluronic block copolymers poly(propylene oxide)-*block*-poly(ethylene oxide)-*block*-poly(propylene oxide) (P123, M_w = 5800, $EO_{20}PO_{70}EO_{20}$, and F127, M_w = 12600, $EO_{106}PO_{70}EO_{106}$) were purchased from Aldrich Corp. Phenol (AR), tetraethyl orthosilicate (TEOS) (AR), ethanol and concentrated ammonia solution (28 wt %), tetrahydrofuran (THF), hydrochloric acid, hexahydrated ferric trichloride ($FeCl_3{\cdot}6H_2O$), trisodium citrate, ethylene glycol, sodium acetate, and sodium hydroxide were purchased from Shanghai Chemical Corp. Millipore water was used in all experiments. Resol, a soluble phenolic resin with low molecular weight (~500 g/mol), was prepared according to previous report[57] and dissolved in ethanol to form a solution with a resol concentration of 20 wt %. For microcystin removal experiments, α-cyano-4-hydroxycinnamic acid (CHCA), acetonitrile (ACN) and trifluoroacetic acid (TFA) were purchased from Merck (Darmstadt, Germany) and aqueous solutions were prepared using Milli-Q water by Milli-Q system (Millipore, Bedford, MA). Microcystin-LR (purity ≥96%) was purchased from Alexis Corporation (San Diego, CA).

2.2. Fabrication of 3DOMC and Magnetic 3DOMC. For the fabrication of 3DOMC, monodisperse silica spheres with different sizes (400 ± 20, 500 ± 20 nm) were synthesized by using Stöber method.[58] After washing with six cycles of centrifugation/redispersion using 5.0 mL of an ethanol/water mixture (50/50 volume ratio), the silica microspheres were then redispersed in ethanol to form a homogeneous solution (10 wt %) for sedimentation for 4 days. After the sedimentation, the supernatant liquor was removed and the remained colloidal crystals were further dried at 30 °C for 12 h and then annealed at 100 °C for 12 h. After that, an ethanolic solution of resol precursor was cast dropwise on small plates of the colloidal crystals. After the evaporation of ethanol for 12 h at 30 °C, the dried monolith was heated in an oven at 100 °C for 6 h for solidifying the resol. The obtained silica/phenolic resin composite was carbonized at 600 °C for 3 h under nitrogen atmosphere using a 3 °C/min ramping rate. The resultant silica/carbon composite was socked in a solution of hydrofluoric acid (4%) for 24 h to etch the silica spheres, followed by washing with water and ethanol three times. The obtained 3DOMC was dried at 50 °C in vacuum overnight. The 3DOMC sample with micrometer-sized macropores[59] was prepared following the similar procedure except that uniform polystyrene colloids of ~1.5 μm were used as the building block of colloidal crystals, and they were removed by pyrolysis at 600 °C at the final step.

For the magnetic 3DOMC with trapped magnetite particle (200 ± 20 nm) in each macropore, the fabrication procedure was similar to that for 3DOMC, except for the uniform core−shell $Fe_3O_4@SiO_2$ microspheres (400 ± 20 nm) used as the building blocks for colloidal crystals, and the silica was etched from the $Fe_3O_4@SiO_2$/carbon composites in a sodium hydroxide solution (2 M) at 70 °C for 6 h.

2.3. Synthesis of Mesoporous Silica Spheres, Hemispheres, and Hollow Spheres. For the synthesis of the mesoporous silica spheres, a stock solution of precursor was first prepared as follows: 1.0 g of Pluronic P123 was dissolved in a mixture consisting of 0.06 g of hydrochloric acid (2 M), 0.9 g of water, and 14 g of ethanol under stirring. Into the obtained clear solution, 2.08 g of TEOS was added, and the solution was further stirred for 1 h to form the precursor solution which is usually used for synthesis of ordered mesoporous silica SBA-15. For convenience, we name it as SBA-15 precursor solution. Three small pieces of 3DOMC plates (1 cm × 1 cm × 0.5 cm, 2.3 g in total) were soaked in the precursor solution for 24 h at 30 °C, and during this period, ethanol was allowed to evaporate simultaneously. After that, the transparent layer on the top of 3DOMC plates was carefully scraped off, and the impregnated 3DOMC composite was placed a Teflon-lined stainless-steel autoclave (30 mL in capacity) containing 10 mL of HCl solution (1.0 M) for hydrothermal treatment (HT) at 100 °C for 10 h. Afterward, the composite was washed with ethanol, dried in vacuum, and was finally calcined in air at 550 °C for 6 h to remove P123 copolymers and 3DOMC.

For the synthesis of mesoporous silica hemispheres, the procedure was similar to that for mesoporous silica spheres. The only difference was that the amount of SBA-15 precursor solution was reduced by 50% and used for soaking the 3DOMC materials.

For the synthesis of mesoporous silica hollow spheres, 3DOMC materials were soaked in the same precursor solution for 2 h, and then taken out to evaporate ethanol for 24 h, followed with similar post-treatment, including the hydrothermal treatment and calcination in air.

2.4. Synthesis of Core−Shell Magnetic Mesoporous Silica Spheres. Small pieces of the sample Fe_3O_4@3DOMC were loaded in a round-bottom flask, and the flask was vacuum pumped to generate reduced pressure. After that, a precursor solution (prepared by mixing 0.1 g of P123, 0.06 g of hydrochloric acid (2 M), 0.9 g of distilled water and 8.0 g of THF for 1 h) was injected into the flask with a syringe. After the samples were soaked in the precursor solution for 5 min in the flask, the flask was open to air for evaporation of THF under 30 °C for 24 h. The impregnated composite was calcined at 550 °C for 6 h in air to burn out P123 copolymers and carbon frameworks.

dx.doi.org/10.1021/ja4099356 | J. Am. Chem. Soc. 2014, 136, 1884−1892

The obtained products were then dispersed in ethanol, and a magnet was used to collect the magnetic mesoporous silica spheres.

2.5. Measurement and Characterization. Transmission electron microscopy (TEM) measurements were carried on a JEOL 2011 microscope (Japan) operated at 200 kV. Scanning electron microscopy (SEM) experiments were conducted on a Philips XL30 electron microscopy operated at 20 kV. Field-emission scanning electron microscopy (FE-SEM) experiments were conducted on the Hitachi model S-4800 field emission scanning microscope. The acquisition of the tilt series for electron tomography (ET) technique was performed on an FEI Tecnai F30 transmission electron microscope operating at 300 kV. All TEM images tilted from −60° to +60° for tilted movie were digitally recorded at a given defocus in a bright-field mode. The cross-sectional TEM specimens were prepared using ultramicrotome (Leica ultracut 63), and the thickness of the section was about 20 nm. Small angle X-ray scattering (SAXS) patterns were collected on a Nanostar U small-angle X-ray scattering system (Bruker, Germany) employing Cu Kα radiation (40 kV, 35 mA). The d-spacing values were calculated using the formula $d = 2\pi/q$. Wide-angle X-ray diffraction (XRD) patterns were recorded on a Bruker D8 powder X-ray diffractometer (Germany) with Ni-filtered Cu Kα radiation (40 kV, 40 mA). Nitrogen adsorption−desorption isotherms were tested at 77 K with a Micromeritics Tristar 3020 analyzer. The samples were degassed under vacuum at 180 °C for at least 6 h before measurements. The specific surface areas were calculated using the Brunauer−Emmett−Teller (BET) method. The pore volumes and pore size distributions were obtained by using the Barrett−Joyner−Halenda (BJH) model from the adsorption branches of isotherms. The total pore volumes (V) were evaluated according to the adsorbed amount at a relative pressure P/P_0 of 0.995.

3. RESULTS AND DISCUSSION

Monolithic colloidal crystals can be easily fabricated via the gravimetric sedimentation of monodisperse colloids of silica microspheres. Through annealing at an elevated temperature, colloidal crystals of silica colloids with a good mechanical stability can be obtained due to the cross-linking of silanol groups on the adjacent silica spheres. Figure 1a shows the typical SEM image of closely packed silica colloidal crystals using uniform silica spheres of around 500 nm as building blocks. Figure 1b shows the 3-D ordered macroporous carbon (3DOMC) replica with uniform cavities of ∼475 nm obtained after the resol infiltration, carbonization, and etching silica templates. The macropore window connecting the cavities is estimated to be about 90 nm in diameter. After a complete impregnation with the precursor solution, followed with solvent evaporation and calcination in air, ordered arrays of uniform mesoporous silica spheres with a diameter of about 450 nm can be obtained (Figure 2a), indicating a faithful replication of the ordered structure of 3DOMC. Interestingly, from the SEM image, several craters can clearly be observed to be regularly distributed in the spheres' surface. It is closely related with the macropore windows of the 3DOMC template. The magnified

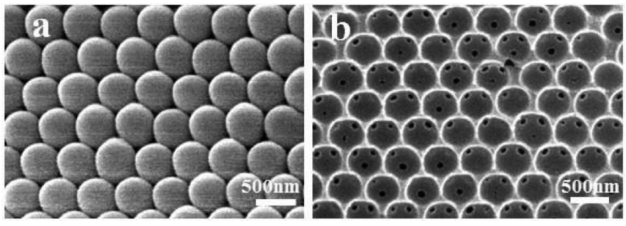

Figure 1. SEM images of (a) the colloidal crystal arrays using uniform silica spheres of ∼500 nm as building blocks and (b) the 3-D ordered macroporous carbon (3DOMC).

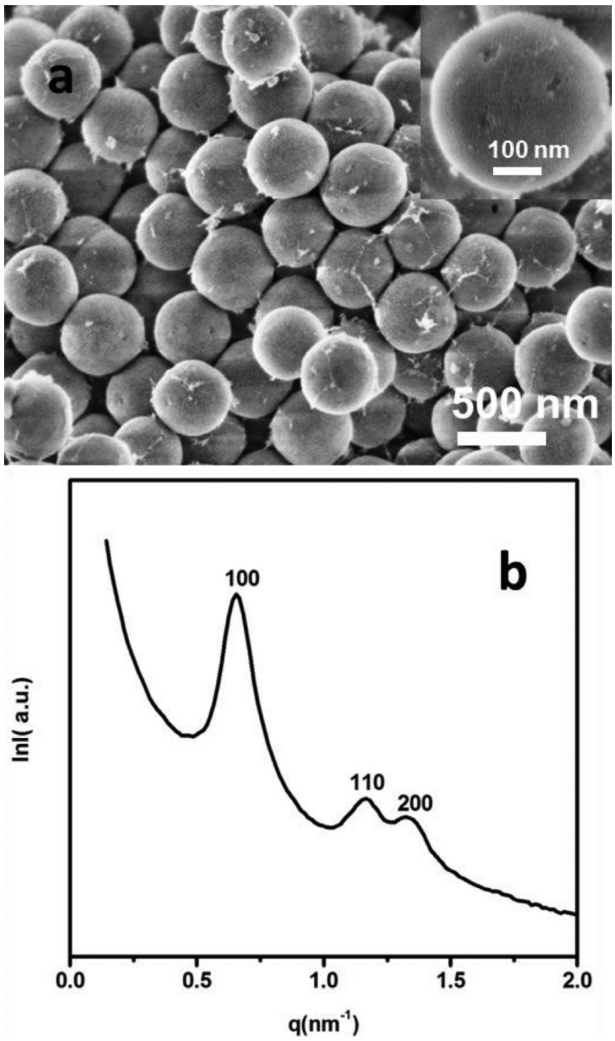

Figure 2. (a) FESEM image and (b) SAXS pattern of the mesoporous silica SBA-15 spheres synthesized via the IDCA approach using P123 as the template. The inset in (a) is the magnified FESEM image.

FESEM image clearly shows the ordered stripe-like mesopores in the spheres' surface (Figure 2a, inset). From the FESEM image of the partially broken microspheres after grinding (Figure S1), it can be seen that the mesopores are circularly arranged in both the surface and inner part of the sphere. SAXS patterns of the sample (Figure 2b) display three well-resolved diffraction peaks at q-value of 0.668, 1.152, 1.322 nm^{-1}, which can be exactly indexed to the 100, 110, and 200 reflections of 2-D hexagonal reflection of 2-D hexagonal mesostructure with a space group of *P6m*, similar to that of SBA-15. Therefore, the sample can be named as SBA-15 spheres.

The TEM image clearly reveals that the obtained mesoporous silica spheres have uniform size, highly ordered mesopores, and typical stripe-like and spherical mesopores can be seen in different domains of individual sphere (Figure 3a−c). The distance between two adjacent stripe-like channels is measured to be ∼9.4 nm, corresponding to the d_{100} spacing. To further gain insight about the pore orientation in a single microsphere, the mesoporous silica spheres were sliced for TEM characterization. As can be seen in the TEM image, the mesopores inside the mesoporous spheres are exclusively concentric circular channels (Figure 3d), in good agreement with the SEM image (Figure S1). To further investigate the

dx.doi.org/10.1021/ja4099356 | J. Am. Chem. Soc. 2014, 136, 1884−1892

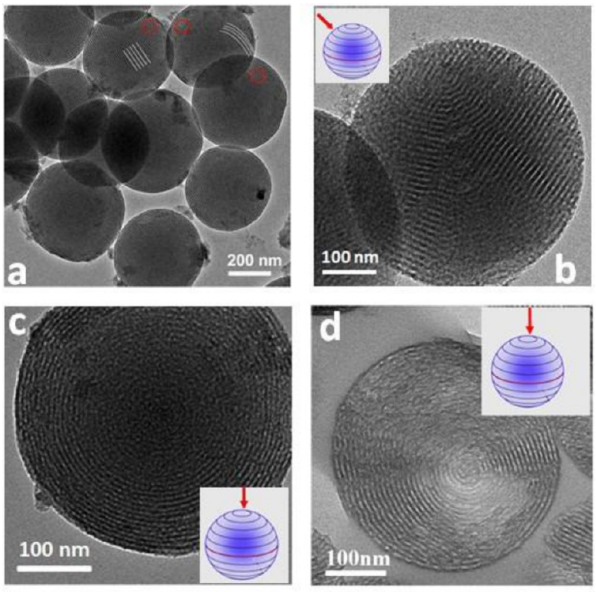

Figure 3. TEM images of the obtained mesoporous silica SBA-15 spheres (a–c) before and (b) after ultrathin microtomming. The insets in (b–d) are the corresponding observing orientation for the ordered mesopores.

internal pore architecture of the mesoporous silica spheres, the electron tomography (ET) technique[60] was performed (Movie S1, Supporting Information). For a selected mesoporous silica microsphere, a series of tilted TEM images ranging from −60° to +60° at an interval of 1° were digitally acquired, and the movie clearly indicate that both hexagonal and stripy mesopores channels can be visible at different tilting angles. These results suggest that, through the coassembly of the block copolymer P123 and silica precursors in the confined macropores of hydrophobic 3DOMC, the mesostructured composites are well-shaped, leading to highly ordered mesoporous silica SBA-15 spheres with unique pore orientation. N_2 adsorption-desorption isotherms of the obtained mesoporous silica SBA-15 spheres exhibit representative type IV curves with a sharp capillary condensation step in the relative pressure range of 0.705–0.80, indicative of large and uniform mesopores (Figure 4a). The slightly deteriorated desorption curve is attributed to the cured mesopore channels of the mesoporous silica spheres. The pore size distribution derived from the adsorption branch of the isotherms using BJH method reveals a uniform mesopore of about 8.0 nm (Figure 4b). The surface area and pore volume of the mesoporous silica

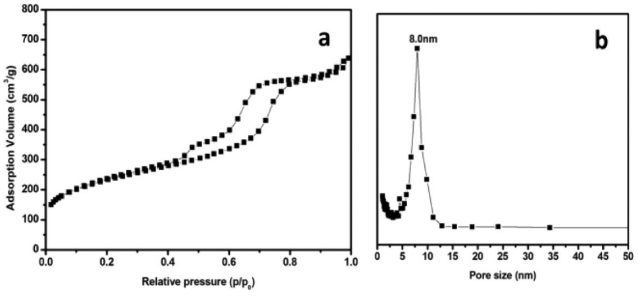

Figure 4. Nitrogen adsorption–desorption isotherms (a) and pore size distribution (b) of the obtained mesoporous silica SBA-15 spheres synthesized via the IDCA approach using P123 as the template.

spheres are calculated to be 790 m^2/g and 0.98 cm^3/g, respectively, which are comparable with typical mesoporous silica SBA-15 samples. Notably, through the same synthesis procedure, the diameter of the mesoporous silica spheres can be readily tuned by changing the macropore size of the 3DOMC. For example, when we employ the 3DOMC with a macropore size of ∼350 nm as the sacrificial host (Figure S2), the uniform mesoporous silica SBA-15 spheres with a diameter of ∼335 nm and similar pore orientation can be obtained, as evidenced by the SEM (Figure S3) and TEM characterizations (Figure S4). With the use of 3DOMC with larger macropores of 1.4 μm[58] as the host reactor (Figure S5a), micrometer-sized mesoporous silica SBA-15 spheres with diameter of about 1.2 μm are synthesized (Figure S5b).

Notably, through the same synthesis procedure with FDU-12 precursor (prepared via the same procedure for SBA-15 precursor but replacing P123 with F127), mesoporous silica spheres with 3-D cubic arrangement of spherical mesopores (*Fm*3*m* space group) can be synthesized. As shown in the SEM image of the mesoporous silica FDU-12 spheres synthesized using hydrophobic 3DOMC with a macropore size of ∼450 nm, the obtained spheres are highly uniform in size and morphology (Figure S6a). And the well-ordered mesopores can be clearly visible in their surface (Figure S6a, inset). The TEM observation further indicates the ordered arrays of spherical mesopores of about 8.0 nm (Figure S6b). The SAXS pattern (Figure S7) reveals three scattering peaks which can be assigned to the 111 and 220 and 311 planes of 3-D cubic mesostructure (*Fm*3*m*). Nitrogen adsorption–desorption isotherms (Figure S8a) of the mesoporous silica FDU-12 spheres exhibit type IV curves with a sharp capillary condensation at capillary condensation step in the relative pressure range of 0.65–0.75. It indicates the presence of uniform large mesopores. The pronounced large H2-type hysteresis loop with delayed capillary evaporation located at a relative pressure of about 0.5 suggests the formation of large caged mesopores with small window size (<5.0 nm). The pore size distribution curve indicates that the obtained FDU-12 spheres have uniform pore size of about 7.4 nm (Figure S8b).

More interestingly, through simply reducing the amount of the precursor solution by 50% for the soaking of the 3DOMC materials (with a macropore size of ∼475 nm), the mesoporous silica particles with unique hemisphere shape can be obtained (Figure 5a). The diameter of the particles is measured from the SEM image to be about 450 nm, close to the macropore size of the 3DOMC host, suggesting that the macropores are almost half filled with the precursor solution. It is worth noting that there is a thin layer spreading upward from the plane of the hemispheres at their edges (marked by the arrows in Figure 5a), and such an intriguing morphology of the mesoporous silica SBA-15 particles has never been reported before. The TEM observation (Figure 5b) also reveals the presence of protuberant edges around the plane of the mesoporous silica hemispheres, which is consistent with the SEM results. The yield of hemispheres is about 90% according to the SEM and TEM observations. Moreover, similar to the above-mentioned mesoporous silica SBA-15 spheres, the silica hemispheres possess concentric circular pore channels, indicative of similar formation process occurred in the two cases. These results clearly indicate that, by simply decreasing the amount of the precursor solution, the macropores of 3DOMC template can be partially or completely filled by the precursor solution, leading to the mesoporous silica particles with tunable morphologies.

dx.doi.org/10.1021/ja4099356 | J. Am. Chem. Soc. 2014, 136, 1884–1892

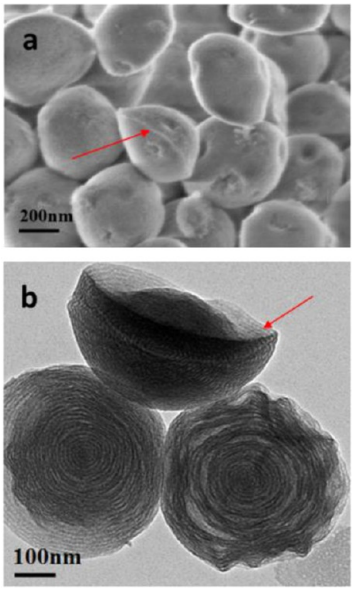

Figure 5. SEM (a) and TEM (b) images of the mesoporous silica (SBA-15) hemispheres. The red arrows indicate the protuberant boarder in the hemispheres generated due to the adsorption of the precursor on the macropore walls.

To further investigate the coassembly process in the confined space, the 3DOMC host materials were soaked in SBA-15 precursor solution for only 2 h and taken out for evaporation of ethanol and calcination in air. Uniform hollow mesoporous silica spheres with a diameter of about 450 nm were obtained. Due to the low amount of the precursor introduced in the macropores, the hollow mesoporous silica spheres formed on the curved surface have a nonuniform morphology and very thin wall (about 50 nm) with poor mesostructure ordering (Figure S9a), which is inferior to hollow mesoporous silica spheres template by discrete polymer latex;[61] however, well-defined stripe-like mesopores of about 8.0 nm can be clearly visible in the wall of the hollow mesoporous silica sphere (Figure S9b). By controlling the concentration of the precursor solution or changing the soaking duration, the thickness of the mesoporous silica shells can be varied in the range of 30−100 nm, with cavity size ranging from 390 to 250 nm. Owing to their tunable wall thickness and cavity size, the mesoporous silica hollow spheres hold great promise for controllable adsorption and release of guest molecules in various applications such as drug release and disease-related peptides or proteins.

On the basis of the above-mentioned results, we propose an interface-directed coassembly (IDCA) mechanism for the formation of mesoporous silica nanostructure confined in the macroporous carbon materials. Taking mesoporous silica SBA-15 sphere as an example (Scheme 1A), when hydrophobic 3DOMC is used as the host materials, all the macropores acting as uniform compartments can be completely filled with precursor solution, when the amount of precursor solution is introduced in excess (step 1). In the course of ethanol evaporation, the silica oligomers formed by the hydrolysis and condensation of TEOS can associate with P123 molecules via hydrogen bonding,[62,63] and further cooperatively assemble into rod-like composite micelles (step 2). The composite micelles can nucleate and further grow on the macropore wall at the solid−liquid interface where the concentration is sharply increased due to rapid evaporation of ethanol in the meniscus. And due to the confinement of the macropores, the composite rod-like micelles adapt a curved morphology and assemble into 2-D hexagonal mesostructure in the same direction along the macropore walls (step 3). With the continuous evaporation of ethanol, the precursor solution around the 3DOMC particles can flow into the macropores driven by the capillary force via macropore windows, and thus, the whole macropores can be completely filled with silica-P123 nanocomposites after the coassembly process. Finally, ordered mesoporous silica spheres with circularly arranged mesopore channels can be obtained after the removal of P123 and carbon frameworks via calcination in air (step 4). As to the mesoporous silica hemispheres, the formation process is slightly different (Scheme 1B). With the evaporation of ethanol, the volume of precursor solution in macropores is dramatically decreased because no sufficient amount of bulk precursor solution of precursor flows into the macropores. In the late period of solvent evaporation, the solution became thick, and at the solid−liquid interface, the sticky precursor can be adsorbed on the macropore wall, leading to a thin layer of ordered mesostructured composites made of curved rod-like P123-silica micelles; meanwhile, the remaining solution in the macropores is continuously concentrated upon ethanol evaporation, which causes the formation of uniform mesostructured composite particles with hemisphere morphology in the macropores. After calcination in air, the 3DOMC and P123 can be burned out, leaving mesoporous silica hemispheres with a thin mesoporous layer spreading upward from the plane at their edge.

The formation of the mesoporous silica hollow spheres is quite simple because no bulk precursor solution is involved. When the 3DOMC materials are soaked in the precursor solution for 2 h and are taken out for evaporation of ethanol, the macropore wall can be coated with a layer of precursor solution due to adsorption. A thin layer of mesostructured P123−silica composites can be in situ formed after evaporation of ethanol. However, due to the effect of gravity, the wall of the macroporous carbon scaffold is not uniformly coated by P123−silica composites. The upper parts of the hollow cavities are coated by thinner composite layer, while the bottom parts are coated by thicker layer. Therefore, after calcination for removal of F127 and 3DOMC template, the upper parts of the replicated mesoporous silica hollow spheres are easier to be broken during sample preparation (grinding or ultrasonication treatment) for SEM observation due to their poor mechanical stability.

By the utilization of the confined self-assembly strategy in 3DOMC materials, mesoporous nanostructure with multi-components and integrated functionalities can be synthesized. In this regards, we designed a procedure for the fabrication of magnetic mesoporous silica SBA-15 nanocomposite by using Fe_3O_4@3DOMC materials where there is one magnetite particle in every macropore (Scheme 2). Monodisperse Fe_3O_4@SiO_2 spheres can be synthesized by coating Fe_3O_4 particles (180 nm) with a layer of silica through a sol−gel coating method.[64] TEM characterization indicates that the obtained core−shell spheres have a silica shell of about 110 nm in thickness (Figure S10a). As revealed by SEM images, they can assemble into highly ordered colloidal crystal through gravimetric sedimentation (Figure S10b). After further infiltration of resol solution, carbonization of resol, and removal of silica, novel magnetic macroporous carbon (Fe_3O_4@3DOMC) materials are obtained. As shown in the SEM

dx.doi.org/10.1021/ja4099356 | J. Am. Chem. Soc. 2014, 136, 1884−1892

Scheme 1. (A) The Formation Mechanism of the Uniform Mesoporous Silica SBA-15 Spheres in the Macropores of 3DOMC Materials; (B) the Formation Process of Hemispherical SBA-15 Materials[a]

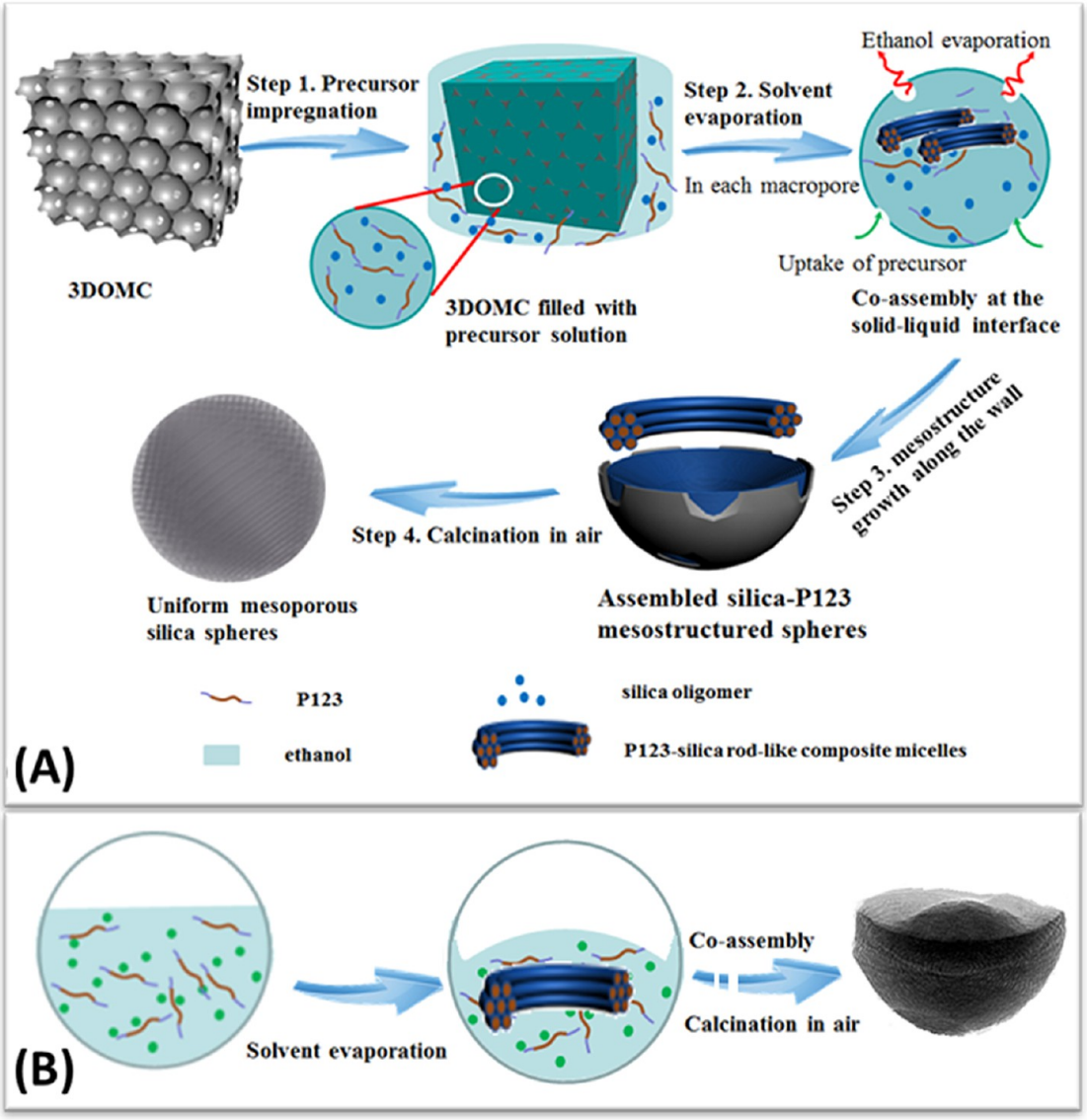

[a](A) The formation mechanism of the uniform mesoporous silica SBA-15 spheres in the macropores of 3DOMC materials, in which the monolithic 3DOMCs are first impregnated by excess amount of the precursor solution, and every macropore is completely filled (step 1). With the evaporation of the solvent, rod-like composite micelles begin to assembly in the macropore; meanwhile, precursor solution in the outside continues to enter into the cavity driven by the capillary force (step 2). As a result, the macropores are completely filled with Pluronic P123−silicate oligomer mesostructured composites after solvent evaporation (step 3). After calcination in air, both carbon framework and Pluronic P123 template can be removed, yielding uniform mesoporous SBA-15 sample. (B) The formation process of hemispherical SBA-15 materials. The 3DOMCs are first partially filled with precursor solution. With the evaporation of ethanol, the solution became thick, and the sticky precursor can be adsorbed on the macropore walls, leading to uniform mesostructured composite particles with hemisphere morphology in the macropores. After calcination in air, the 3DOMC and P123 can be burned out, leaving mesoporous silica hemispheres with a thin mesoporous layer spreading upwards from the plane at their edge.

image, uniform macropores with large windows (ca. 30 nm) are aligned in 3-D ordered arrays, and single Fe_3O_4 particle can be clearly seen in the macropores (Figure S11). Notably, it is the first time that such a unique Fe_3O_4@3DOMC structure has been fabricated through the core−shell sphere templating approach, and the magnetic 3DOMC may find applications for magnetic sensing and so on. After impregnation with the SBA-15 precursor solution and evaporation of solvent, the macropores can be completely filled, and the Fe_3O_4 particles in the macropores can be in situ coated by the resulting P123-silica mesostructured composite due to the excellent surface affinity of iron oxide toward silica species. After calcination, magnetic mesoporous silica (magnetic SBA-15) spheres are obtained. As shown in Figure 6, Fe_3O_4 particles are successfully coated by mesoporous silica, yielding uniform heterostructured composite spheres with a diameter of about 400 nm, and mesopore channels can be clearly visible in the magnified TEM image (Figure 6, the inset in the upper right corner). The magnetic mesoporous silica SBA-15 spheres can be easily dispersed in an aqueous solution (0.1 mg/mL). With the use of

dx.doi.org/10.1021/ja4099356 | J. Am. Chem. Soc. 2014, 136, 1884−1892

Scheme 2. The Synthesis Route for Uniform Magnetic Mesoporous Silica SBA-15 Spheres in the Macropores of the Magnetic 3DOMC Materials Which Possess a Magnetic Particle in Each Macropore

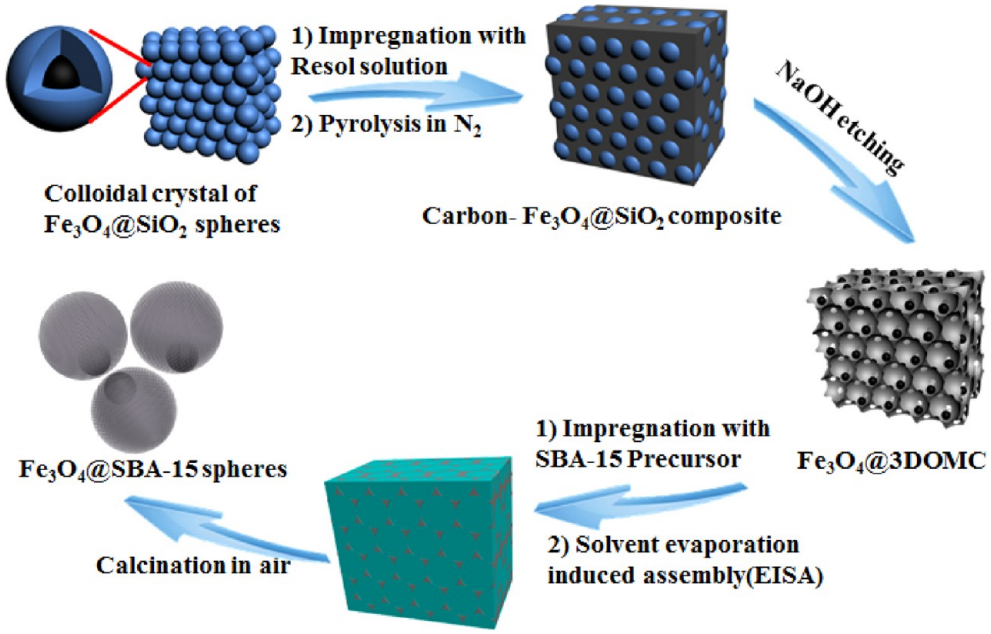

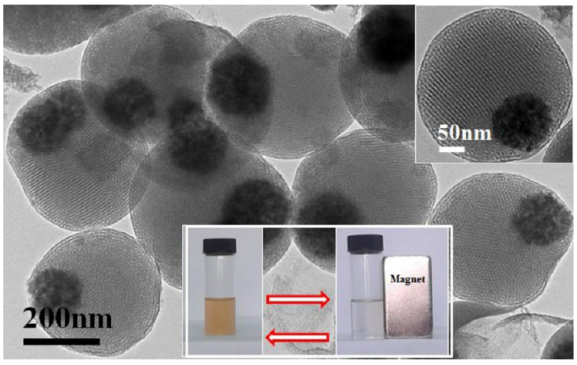

Figure 6. The TEM image of the magnetic mesoporous silica (magnetic SBA-15) spheres. The inset in the upper right corner is the magnified TEM image. The inset at the bottom shows the separation and redispersion of the magnetic SBA-15 spheres in water.

a magnet (~4000 Oe), a fast separation of magnetic SBA-15 spheres can be achieved in ca. 60 s, and they can be quickly redispersed in the solution after removal of the applied magnetic field (Figure 6, inset in the bottom). The excellent magnetic responsivity of the magnetic SBA-15 spheres is favorable for their applications as absorbents and/or carriers of guest molecules. Magnetic property characterization (Figure S12) using Superconducting quantum interference device (SQUID) indicates that the obtained magnetic SBA-15 spheres exhibit a superparamagnetic property at room temperature, i.e., no remanence is detected after removal of magnetic field, and the saturated magnetization value is calculated to be 23.5 emu/g, implying a relatively high content of magnetic component. Wide-angle XRD measurements reveal that the obtained magnetic SBA-15 spheres display well resolved diffraction patterns similar to those of Fe_3O_4 particles (Figure S13). It implies that the structure of magnetite particles is well-retained in the whole synthesis process. The nitrogen adsorption–desorption measurement (Figure S14) reveals that the obtained Fe_3O_4@SBA-15 spheres have uniform mesopore size of about 7.0 nm, BET surface area of 280 m^2/g, and total pore volume of 0.404 cm^3/g.

The high surface area and good magnetic responsivity of the obtained Fe_3O_4@SBA-15 spheres make them a good candidate for application in the removal of harmful organics in water. Microcystin (MC) is a family of cyclicheptapeptide toxins with a hydrodynamic molecular dimension of 2–3 nm. Removal of MCs is a big challenge because they are highly water-soluble. In the MC family, the microcystin MC-LR (Figure S15a) is frequently tested as a marker for cyanobacteria occurrence. Therefore, in this study MC-LR is used as a model compound for evaluation of adsorption performance of the magnetic SBA-15 spheres. The standard curve (Figure S15b) was obtained by measurement of a series of MC-LR solutions (0.1–100 μg/L). Figure S16 shows the MALDI-TOF-MS spectrum of MC-LR solution (100 μg/L, 100 μL) before and after treatment with 0.6 mg of the Fe_3O_4@SBA-15 spheres. The signal intensity (S/N) of MC-LR at ~990 m/z is significantly reduced from ~1921 to ~310, accounting for a high removal rate of 84%. To obtain an optimized addition amount of the magnetic SBA-15 spheres, various amounts of the absorbent from 0 to 3.0 mg were used for adsorption of MC-LR (100 μg/L, 100 μL). With the increase of absorbent amount, the signal intensity of MC-LR in the residual solution decreases dramatically from the initial value of 1921 to 18.2 with 2.0 mg of the absorbent, and further increase of the addition only leads to minor decrease of MC-LR concentration (Figure S17). Therefore, the addition amount of 2.0 mg is an optimized value. Furthermore, the removal efficiency versus the adsorption time was investigated because the adsorption time (i.e., the incubation duration) is also an important parameter in practical application. It was found that the signal intensity of residual MC-LR is quickly decreased from the initial value of 1921 to 81.8 in the first 5 min and to 18.2 at 10 min, and at 15 min, it decreases to 15.0, corresponding to a removal efficiency of about 99.3% with a MC-LR concentration of 0.7 μg/L, lower than that for the drinking-water standard (1.0 μg/L) proposed by WHO (Figure S18). Prolonging the adsorption time to 30 min hardly reduces

dx.doi.org/10.1021/ja4099356 | J. Am. Chem. Soc. 2014, 136, 1884–1892

the signal intensity of MC-LR in the solution. Therefore, an incubation time of 15 min is sufficient for an efficient removal of MC-LR using the magnetic SBA-15 spheres. Notably, the magnetic SBA-15 spheres can be readily recycled via magnetic separation. The recycled absorbent can be regenerated by extraction with acetonitrile, and no significant decrease of the removal efficiency for MC-LR is observed even after the use for 10 times (Figure S19), indicating an excellent performance of the magnetic absorbent in removing the toxic MC-LR in water.

4. CONCLUSIONS

In summary, an effective interface-directed coassembly strategy has been developed for the synthesis of monodisperse mesoporous silica particles with a large pore size (ca. 8 nm) by using 3-D ordered macroporous carbon (3DOMC) as the nanoreactor for the confined solvent evaporation induced coassembly of template molecules and silica source. The morphology of mesoporous silica particles (spheres, hollow spheres, and hemispheres) can be controlled by the amount of precursor solution introduced into the macropore cavities, and the particle size is tunable from submicrometer to micrometer regimes by changing the macropore diameter of 3DOMC. The structure of mesoporous silica spheres can be varied from 2-D hexagonal (*P6m*) to 3-D face centered cubic symmetry (*Fm3m*) by using different Pluronic copolymers as structure-directing agents. With this strategy, by preplacing a magnetic particle in each macropore of the 3DOMC template before introducing precursor solutions, novel composite mesoporous silica spheres with a magnetic core and mesoporous silica shell can be obtained. As a result of high magnetization (23.5 emu/g) and high surface area (280 m^2/g), the magnetic mesoporous silica spheres show a fast and efficient (99.3%) removal of microcystin from water. After easy regeneration by solvent extraction, the magnetic absorbent can be recycled for more than 10 times without significant decrease in uptake of microcystin. It is expected that this novel approach can be widely used to synthesize various spherical particles with high porosity, multifunctionalities, and integrated properties for various applications including catalysis, drug delivery, and so forth.

■ ASSOCIATED CONTENT

Supporting Information

The experimental details for removal of microcystins using magnetic SBA-15 spheres as the absorbent; FESEM images of broken SBA-15 spheres; SEM images of 3DOMC template with different macropore size; FESEM and TEM images of SBA-15 spheres with different diameters; FESEM and TEM images, SAXS pattern, N_2 sorption isotherms of FDU-12 spheres; FESEM and TEM images of SBA-15 hollow spheres; TEM images of Fe_3O_4@SiO_2; SEM images of Fe_3O_4@SiO_2 colloidal crystals; SEM images of Fe_3O_4@3DOMC; the magnetization hysteresis loops of the obtained magnetic mesoporous silica SBA-15 spheres; XRD patterns of Fe_3O_4 and magnetic mesoporous silica SBA-15 spheres; N_2 sorption isotherms of magnetic mesoporous silica SBA-15 spheres; the molecular structure of MC-LR; the absorbent data of MC-LR using magnetic mesoporous silica SBA-15 spheres. This material is available free of charge via the Internet at http://pubs.acs.org.

■ AUTHOR INFORMATION

Corresponding Author

yhdeng@fudan.edu.cn

Notes

The authors declare no competing financial interest.

■ ACKNOWLEDGMENTS

This work was supported by the State Key 973 Program of PRC (2013CB934104 and 2012CB224805), the NSF of China (21073040 and 51372041), the specialized research fund for the doctoral program of higher education of China (20120071110007), the innovation program of Shanghai Municipal Education Commission (13ZZ004), Shanghai Rising Star Project of STCSM (12QH1400300), Program for New Century Excellent Talents in University (NCET-12-0123).

■ REFERENCES

(1) Xia, Y. N.; Gates, B.; Yin, Y. D.; Lu, Y. *Adv. Mater.* **2000**, *12*, 693−713.
(2) Gallis, K. W.; Araujo, J. T.; Duff, K. J.; Moore, J. G.; Landry, C. C. *Adv. Mater.* **1999**, *11*, 1452−1455.
(3) Boissiere, C.; Kummel, M.; Persin, M.; Larbot, A.; Prouzet, E. *Adv. Funct. Mater.* **2001**, *11*, 129−135.
(4) Jiang, Z. T.; Zuo, Y. M. *Anal. Chem.* **2001**, *73*, 686−688.
(5) Ma, Y. R.; Qi, L. M.; Ma, J. M.; Wu, Y. Q.; Liu, O.; Cheng, H. M. *Colloids Surf., A* **2003**, *229*, 1−8.
(6) Martin, T.; Galarneau, A.; Renzo, F. D.; Brunel, D.; Fajula, F. *Chem. Mater.* **2004**, *16*, 1725−1731.
(7) Sun, X. M.; Li, Y. D. *Angew. Chem., Int. Ed.* **2004**, *43*, 597−601.
(8) Deng, Y. H.; Cai, Y.; Sun, Z. K.; Liu, J.; Liu, C.; Wei, J.; Li, W.; Liu, C.; Wamg, Y.; Zhao, D. Y. *J. Am. Chem. Soc.* **2010**, *132*, 8466−8473.
(9) Wang, Y. J.; Caruso, F. *Chem. Mater.* **2005**, *17*, 953−961.
(10) Wu, S. G.; Liu, B. L.; Li, S. J. *Int. J. Biol. Macromol.* **2005**, *37*, 263−267.
(11) Holland, B. T.; Blanford, C. F.; Do, T.; Stein, A. *Chem. Mater.* **1999**, *11*, 795−805.
(12) Graf, C.; van Blaaderen, A. *Langmuir* **2002**, *18*, 524−534.
(13) Lai, C.-Y.; Trewyn, B. G.; Jeftinijia, D. M.; Jeftinijia, K.; Xu, S.; Jeftinijia, S.; Lin, V. S. Y. *J. Am. Chem. Soc.* **2003**, *125*, 4451−4459.
(14) Zhu, Y. F.; Shi, J. L.; Shen, W. H.; Dong, X. P.; Feng, J. W.; Ruan, M. L.; Li, Y. S. *Angew. Chem., Int. Ed.* **2005**, *44*, 5083−5087.
(15) Vallet-Regi, M.; Balas, F.; Arcos, D. *Angew. Chem., Int. Ed.* **2007**, *46*, 7548−7558.
(16) Radu, D. R.; Lai, C.-Y.; Jeftinijia, K.; Rowe, E. W.; Jeftinijia, S.; Lin, V. S. Y. *J. Am. Chem. Soc.* **2004**, *126*, 13216−13217.
(17) Slowing, I. I.; Vivero-Escoto, J. L.; Wu, C.-W.; Lin, V. S. Y. *Adv. Drug Delivery Rev.* **2008**, *60*, 1278−1288.
(18) Torney, F.; Trewyn, B. G.; Lin, V. S. Y.; Wang, K. *Nat. Nanotechnol.* **2007**, *2*, 295−300.
(19) Corma, A. *Chem. Rev.* **1997**, *97*, 2373−2419.
(20) Lee, J.; Park, J. C.; Song, H. *Adv. Mater.* **2008**, *20*, 1523−1528.
(21) Mercier, L.; Pinnavaia, T. J. *Adv. Mater.* **1997**, *9*, 500−503.
(22) Zhao, X. S.; Lu, G. Q. *J. Phys. Chem. B* **1998**, *102*, 1556−1561.
(23) Guo, L. M.; Li, J. T.; Zhang, L. X.; Li, J. B.; Li, Y. S.; Yu, C. C.; Shi, J. L.; Ruan, M. L.; Feng, J. W. *J. Mater. Chem.* **2008**, *18*, 2733−2738.
(24) Beck, J. S.; Vartuli, J. C.; Roth, W. J.; Leonowicz, M. E.; Kresge, C. T.; Schmitt, K. D.; Chu, C. T-W.; Olson, D. H.; Sheppard, E. W.; McCullen, S. B.; Higgins, J. B.; Schlenker, J. L. *J. Am. Chem. Soc.* **1992**, *114*, 10834−10843.
(25) Nooney, R. I.; Thirunavukkarasu, D.; Chen, Y. M.; Josephs, R.; Ostafin, A. E. *Chem. Mater.* **2002**, *14*, 4721−4728.
(26) Lin, Y.-S.; Tsai, C.-P.; Huang, H.-Y.; Kuo, C.-T.; Hung, Y.; Huang, D.-M.; Chen, Y.-C.; Mou, C.-Y. *Chem. Mater.* **2005**, *17*, 4570−4573.
(27) Sayari, A. *Angew. Chem., Int. Ed.* **2000**, *39*, 2920−2922.

(28) Jana, S. K.; Nishida, R.; Shindo, K.; Kugita, T.; Namba, S. *Microporous Mesoporous Mater.* **2004**, *68*, 133−142.
(29) Slowing, I. I.; Trewyn, B. G.; Lin, V. S.-Y. *J. Am. Chem. Soc.* **2007**, *129*, 8845−8849.
(30) Kim, M.-H.; Na, H.-K.; Kim, Y.-K.; Ryoo, S.-R.; Cho, H. S.; Lee, K. E.; Jeon, H.; Ryoo, R.; Min, D.-H. *ACS Nano* **2011**, *5*, 3568−3576.
(31) Mizutani, M.; Yamada, Y.; Nakamura, T.; Yano, K. *Chem. Mater.* **2008**, *20*, 4777−4782.
(32) Hanrahan, J. P.; Donovan, A.; Morris, M. A.; Holmes, J. D. *J. Mater. Chem.* **2007**, *17*, 3881−3887.
(33) Tan, B.; Rankin, S. E. *Langmuir* **2005**, *21*, 8180−8187.
(34) Gu, J. L.; Huang, K.; Zhu, X. Y.; Li, Y. S.; Wei, J.; Zhao, W. R.; Liu, C. S.; Shi, J. L. *J. Colloid Interface Sci.* **2013**, *407*, 236−242.
(35) Zhao, D. Y.; Sun, J. Y.; Li, Q. Z.; Stucky, G. D. *Chem. Mater.* **2000**, *12*, 275−279.
(36) Katiyar, A.; Yadav, S.; Smirniotis, P. G.; Pinto, N. G. *J. Chromatogr., A* **2006**, *1122*, 13−20.
(37) Lu, Y. F.; Fan, H. Y.; Stump, A.; Ward, T. L.; Rieker, T.; Brinker, C. J. *Nature* **1999**, *398*, 223−226.
(38) Brinker, C. J.; Lu, Y. F.; Sellinger, A.; Fan, H. Y. *Adv. Mater.* **1999**, *11*, 579−585.
(39) Holland, B. T.; Blanford, C. F.; Stein, A. *Science* **1998**, *281*, 538−540.
(40) Wijnhoven, J. E. G. J.; Vos, W. L. *Science* **1998**, *281*, 802−804.
(41) Blanford, C. F.; Yan, H.; Schroden, R. C.; Al-Daous, M.; Stein, A. *Adv. Mater.* **2001**, *13*, 401−407.
(42) Velev, O. D.; Jede, T. A.; Lobo, R. F.; Lenhoff, A. M. *Nature* **1997**, *389*, 447−448.
(43) Zakhidov, A. A.; Baughman, R. H.; Iqbal, Z.; Cui, C.; Khayrullin, I.; Dantas, S. O.; Marti, J.; Ralchenko, V. G. *Science* **1998**, *282*, 897−901.
(44) Schroden, R. C.; Al-Daous, M.; Blanford, C. F.; Stein, A. *Chem. Mater.* **2002**, *14*, 3305−3315.
(45) Scott, R. W. J.; Yang, S. M.; Chabanis, G.; Coombs, N.; Wiliams, D. E.; Ozin, G. A. *Adv. Mater.* **2001**, *13*, 1468−1472.
(46) Lee, Y. J.; Braun, P. V. *Adv. Mater.* **2003**, *15*, 563−566.
(47) Li, Z. Y.; Zhang, Z. Q. *Phys. Rev. B* **2000**, *62*, 1516−1519.
(48) Yang, S. M.; Coombs, N.; Ozin, G. A. *Adv. Mater.* **2000**, *12*, 1940−1944.
(49) Jiang, P.; Bertone, J. F.; Colvin, V. L. *Science* **2001**, *291*, 453−457.
(50) Chae, W.-S.; Braun, P. V. *Chem. Mater.* **2007**, *19*, 5593−5597.
(51) Miguez, H.; Tetreault, N.; Yang, S. M.; Kitaev, V.; Ozin, G. A. *Adv. Mater.* **2003**, *15*, 597−600.
(52) Kim, S. S.; Shah, J.; Pinnavaia, T. J. *Chem. Mater.* **2003**, *15*, 1664−1668.
(53) Yoo, W. C.; Kumar, S.; Wang, Z.; Ergang, N. S.; Fan, W.; Karanikolos, G. N.; McCormick, A. V.; Penn, R. L.; Tsapatsis, M.; Stein, A. *Angew. Chem., Int. Ed.* **2008**, *47*, 9096−9099.
(54) Mandlmeier, B.; Szeifert, J. M.; Fattakhova-Rohlfing, D.; Amenisch, H.; Bein, T. *J. Am. Chem. Soc.* **2011**, *133*, 17274−17284.
(55) Schuster, J.; He, G.; Mandlmeier, B.; Yim, T.; Lee, K. T.; Bein, T.; Nazar, L. F. *Angew. Chem., Int. Ed.* **2012**, *51*, 3591−3595.
(56) Sun, Z. K.; Liu, Y.; Li, B.; Wei, J.; Wang, M. H.; Yue, Q.; Deng, Y. H.; Kaliaguine, S.; Zhao, D. Y. *ACS Nano* **2013**, *7*, 8706−8714.
(57) Meng, Y.; Gu, D.; Zhang, F. Q.; Shi, Y. F.; Yang, H. F.; Li, Z.; Yu, C. Z.; Tu, B.; Zhao, D. Y. *Angew. Chem., Int. Ed.* **2005**, *44*, 7053−7059.
(58) Stöber, W.; Fink, A.; Bohn, E. *J. Colloid Interface Sci.* **1968**, *26*, 62−69.
(59) Deng, Y. H.; Liu, C.; Liu, J.; Zhang, F.; Yu, T.; Zhang, F. Q.; Gu, D.; Zhao, D. Y. *J. Mater. Chem.* **2008**, *18*, 408−415.
(60) Shen, S. D.; Gu, T.; Mao, D. S.; Xiao, X. Z.; Yuan, P.; Yu, M. H.; Xia, L. Y.; Ji, Q.; Meng, L.; Song, W.; Yu, C. Z.; Lu, G. Z. *Chem. Mater.* **2012**, *24*, 230−235.
(61) Blas, H.; Save, M.; Pasetto, P.; Boissiere, C.; Sanchez, C.; Charleux, B. *Langmuir* **2008**, *24*, 13132−13137.
(62) Zhao, D. Y.; Feng, J. L.; Huo, Q. S.; Melosh, N.; Frefrickson, G. H.; Chmelka, B. F.; Stucky, G. D. *Science* **1998**, *279*, 548−552.
(63) Zhao, D. Y.; Huo, Q. S.; Feng, J. L.; Chmelka, B. F.; Stucky, G. D. *J. Am. Chem. Soc.* **1998**, *120*, 6024−6036.
(64) Deng, Y. H.; Qi, D. W.; Deng, C. H.; Zhang, X. M.; Zhao, D. Y. *J. Am. Chem. Soc.* **2008**, *130*, 28−29.